Solution to the phase problem for specular x-ray or neutron reflectivity from thin films on liquid surfaces

J. Kent Blasie, Songyan Zheng, and Joseph Strzalka
Department of Chemistry, University of Pennsylvania, Philadelphia, Pennsylvania 19104-6323
(Received 25 February 2003; published 5 June 2003)

The phase problem for specular x-ray and neutron reflectivity from liquid surfaces and thin films on liquid surfaces can be solved in the distorted-wave Born approximation. The gradient of the scattering-length density (SLD) profile normal to the plane of the surface is bounded in these cases. This provides a powerful constraint allowing the phase problem to be solved with no *a priori* assumptions via an iterative Fourier refinement procedure applied to the Fresnel-normalized reflectivity. The critical boundary condition can be determined experimentally from the autocorrelation of the gradient profile obtained via an inverse Fourier transform of the Fresnel-normalized reflectivity without phase information. The phase solution and the resulting gradient SLD profile can be shown to be unique, and therefore unambiguously determined, when all of phase space is systematically explored for particular cases, especially for thin films on liquid surfaces. This gradient SLD profile can then be integrated either numerically, or better, analytically to provide the scattering-length density profile itself on an absolute scale.

DOI: 10.1103/PhysRevB.67.224201 PACS number(s): 68.18.Fg

INTRODUCTION

There seems to be a perception that the phase problem for specular x-ray and neutron reflectivity from liquid surfaces, or from thin films on liquid surfaces, either has not or cannot be solved even for cases where the distorted-wave Born approximation is satisfied.[1,2] As a result, most resort to the so-called ''slab-model'' refinement approach.[3] In this approach, one considers the scattering-length density (SLD) profile structure of the monolayer $\rho(z)$ to consist of layers (or ''slabs'') of average density $\overline{\rho_j}$ bounded by the two interfaces z_j and z_{j+1} of widths (or roughnesses) σ_j and σ_{j+1}, which can be conveniently described by a sum of analytic error functions completely defined by these parameters. Here, z is the profile coordinate normal to the plane of the surface and the profile structure $\rho(z)$ is the projection of the three-dimensional (3D) SLD distribution of the monolayer parallel to the plane of the monolayer onto the z coordinate. As a result, the corresponding derivative or gradient profile $d\rho(z)/dz$ can be described by a sum of analytic Gaussian functions, the Gaussian for each interface completely defined by the change in average SLD across the interface $\Delta\rho_{j,j+1}$, its position in the profile z_j, and its width (or roughness) σ_j. Initial models for the SLD profile of the monolayer using this method must be then constructed, based on one's physical-chemical knowledge of the system of interest, and the model then refined against the Fresnel-normalized reflectivity data via

$$R(q_z)/R_F(q_z)=\left|\rho_\infty^{-1}\int (d\rho/dz)\exp(iq'z)dz\right|^2\equiv|F(q_z')|^2, \tag{1}$$

where $R(q_z)$ is the experimental reflectivity (normalized only by the incident beam flux) as a function of momentum transfer q_z normal to the surface, $R_F(q_z)$ is the Fresnel reflectivity from a single infinitely sharp (ideal) interface, the average SLD of the semi-infinite bulk subphase is ρ_∞, q_c is q_z at the critical angle for the subphase α_c, and $q_z'=\sqrt{q_z^2-q_c^2}$. It is well known that the nonlinear least-squares fitting procedures employed in the refinement of the right-hand side of Eq. (1) for the initial model against the experimental Fresnel-normalized reflectivity on the left-hand side necessarily is refined to the gradient profile for the monolayer most similar to the initial model. Thus, given both the potential complexity of many of the monolayer thin film systems of interest today[4,5] and the fact that the SLD profile is the projection of a 3D SLD distribution onto a single axis, the so-called ''slab-model'' refinement method might be viewed as less than totally objective.

Some time ago, it was recognized that the phase problem for the SLD distribution itself could be solved in the first Born approximation and this solution was unique, provided that it was bounded in one, two, or three dimensions and possessed a center of symmetry or antisymmetry, utilizing the power of both constraints.[6] In such cases, the autocorrelation of the SLD distribution is bounded and it can be ''deconvoluted'' via either recursion or Fourier methods.[7,8] For asymmetric SLD distributions, an iterative refinement approach was developed[8–10] that was called ''box refinement,'' where the term ''box'' referred to the boundedness, and the convergence was driven by this constraint. In such cases, the solution was generally not unique, although the systematic exploration of phase space could be used to search for the possibility of other solutions.

It was only recently recognized that the same approach could be applied to specular x-ray reflectivity data from Langmuir monolayers of amphiphiles at the air-water interface, since their gradient SLD profiles are bounded and the distorted-wave Born approximation is satisfied.[11,4] This recent discovery is further elaborated here. It can now be shown to produce a unique solution for particular cases of thin films on liquid surfaces and the same structural parameters defined by the slab-model refinement approach, but unambiguously without any *a priori* assumptions. Somewhat

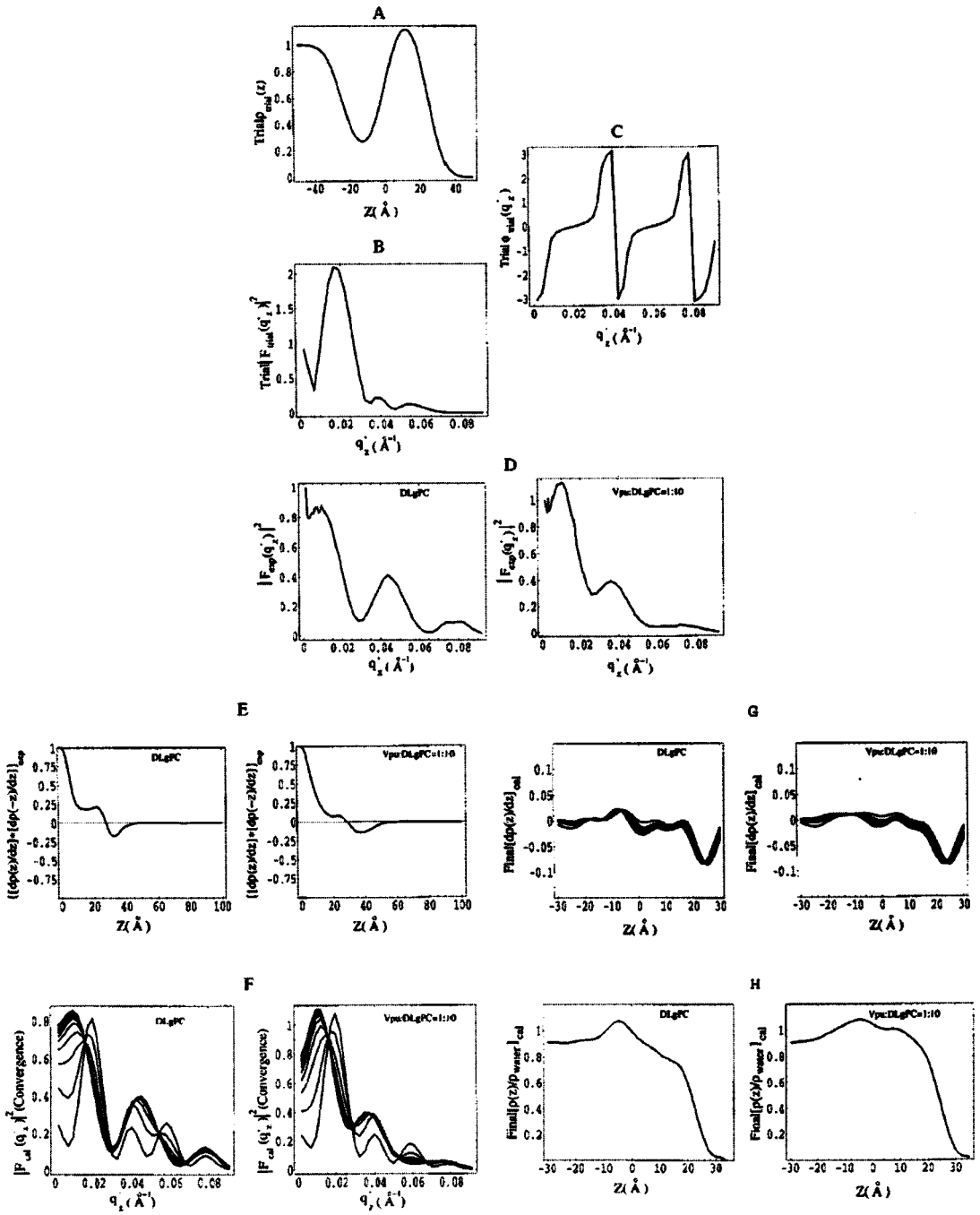

FIG. 1. Illustration of the box-refinement method of analysis for Fresnel-normalized x-ray reflectivity data from Langmuir monolayers of the pure diacylphospholipid DLgPC and its binary mixture with an HIV-1 accessory protein Vpu at a DLgPC/Vpu mole ratio of 10:1. In this and subsequent figures, reciprocal space functions are plotted vs q_z' (Å^{-1}) as defined in the distorted-wave Born approximation (see text), but where $|q_z| = (2 \sin\theta)/\lambda$ instead of $|q_z| = (4\pi \sin\theta)/\lambda$; all real space functions are plotted vs the profile coordinate z(Å). (A) Trial electron density profile $\rho_{trial}(z)$ used to initiate the box refinement. (B) Modulus squared $|F_{trial}(q_z')|^2$ of the Fourier transform of the gradient $[d\rho_{trial}(z)/dz]$ as a function of photon momentum transfer q_z'. (C) Phase $\phi_{trial}(q_z')$ of the Fourier transform of the gradient $[d\rho_{trial}(z)/dz]$ as a function of photon momentum transfer q_z'. Only this trial phase function originating from the trial electron density profile $\rho_{trial}(z)$ is used to initiate the box refinement. (D) Experimental normalized reflectivity $R(q_z')/R_F(q_z')$ expressed as a function of photon momentum transfer q_z', $|F_{trial}(q_z')|^2$. Note that neither case agrees with the modulus squared $|F_{trial}(q_z')|^2$ of the Fourier transform of the gradient $[d\rho_{trial}(z)/dz]$ shown in (B). (E) Inverse Fourier transform of the experimental $|F_{expt}(q_z')|^2$ which provides the autocorrelation of the gradient of the electron density profile $\langle [d\rho_{expt}(z)/dz][d\rho_{expt}(-z)/dz] \rangle$ for the monolayer. The box constraint, key input to the box refinement analysis, was chosen to be $L = 60$ Å, well beyond the last significant feature at $z \approx 40$ Å. (F) The convergence of the calculated $|F(q_z')|^2$ from the box-refinement to the experimental $|F_{expt}(q_z')|^2$ for iterations 1–10, 20, 30, 40, 50. (G) The convergence of the calculated $d\rho(z)/dz$ from the box refinement to the final $d\rho_{expt}(z)/dz$ for iterations 1–10, 20, 30, 40, 50. (H) The numerical integration of the final converged $d\rho(z)/dz$ to the absolute electron density profile for the monolayer $\rho_{expt}(z)$ itself. (This figure reprinted from Ref. 4 with permission of the Biophysical Society.)

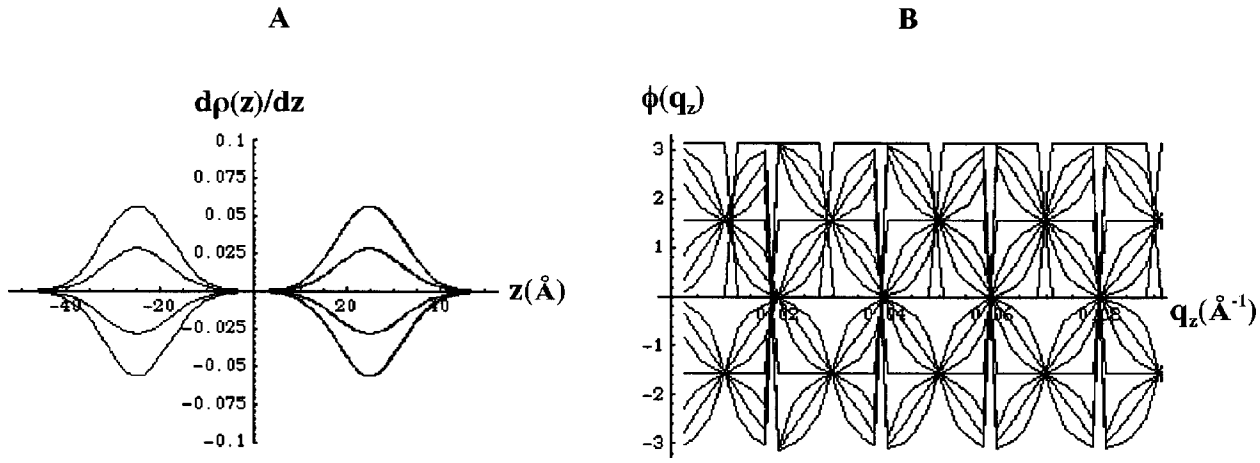

FIG. 2. The q_z-region of phase space accessed in the Fresnel-normalized x-ray reflectivity data shown in Fig. 1 was systematically explored using a finite set of gradient electron density profiles $d\rho(z)/dz$. These were based on all possible combinations of two Gaussian functions, each of five possible amplitudes (e.g., 0, $\pm\Delta$, $\pm 2\Delta$), and separated by 50 Å, the maximum extent of the bounded region in which the experimental gradient profiles are nonzero, thereby providing gradient profiles ranging from totally symmetric (even) to totally antisymmetric (odd) with intermediate asymmetric cases, as shown superimposed in (A). A superposition of the phase functions $\phi(q_z)$ of the Fourier transforms $F(q_z')$ of this set of gradient profiles, shown in (B), demonstrating their adequacy in searching the available phase space over this range of momentum transfer q_z accessed.

earlier, Clinton[12] showed that for such bounded gradient SLD profiles, a unique analytic solution to the phase problem could be provided via the logarithmic dispersion relations for Fourier transforms.[13] However, the restrictions placed on the $\Delta\rho_{j,j+1}$'s and the σ_j's sufficient for a unique solution [namely when $F(q_z')$ in Eq. (1) contains no zeros in the upper half complex q plane or on the real axis) were such that the greatest applicability occurs for the case of inorganic multilayer films in which the SLD contrast could be controlled, i.e., the magnitudes of the $\Delta\rho_{j,j+1}$'s, and the interfacial roughnesses, i.e., the σ_j's, could be made small, via their fabrication. This approach was extended[14] to cases not satisfying these severe restrictions [namely, when $F(q_z')$ in Eq. (1) contains a finite number of zeros in the upper half complex q plane or on the real axis] by using an approximate phase solution, treating the correction to the analytic phase solution provided by the logarithmic dispersion relations as a perturbation (i.e., small) that could be solved iteratively. However, this perturbation approach ultimately resulted in the requirement that a portion of the SLD profile be known independently, making it equivalent to ''interferometry.'' The more powerful interferometric approach to solving the phase problem for thin films on the surfaces of inorganic substrates, employing the latter as the reference SLD profile, has been implemented via both iterative Fourier refinement methods in the first Born and distorted-wave Born approximations[15,16] and direct analytic inversion.[17,18] The latter analytic inversion requires two different reference structures for the same thin film, unless ferromagnetic effects in the reference structure can be utilized to alter its effective SLD profile in the case of spin-dependent neutron reflectivity. However, the requirement for a reference structure in close apposition to the thin film of interest, in the case of interferometric phasing, may well present an unacceptable perturbation of the latter structure. More generally, the box-refinement approach should be applicable to any interfacial system for which the profile projection as defined can be considered to be effectively constant outside some region along the profile axis, and hence its gradient profile is bounded or zero outside the boundaries defining this region. However, for some systems, e.g., for sufficiently thick films, the extent of the gradient profile may become too large, thereby limiting the available reflectivity data to a range of momentum transfer where the distorted-wave Born approximation may not be valid.[1]

METHODS

The box-refinement method as implemented via Eq. (1) for x-ray reflectivity from a liquid surface was fully described in Ref. 4. Briefly, the inverse Fourier transform of the Fresnel-normalized reflectivity itself is used to produce uniquely the autocorrelation of the gradient profile. Since the gradient profile is bounded, the amplitudes of the fluctuations in its autocorrelation decay with increasing shift parameter to a minimal level at, and remain so beyond, the boundary for both positive and negative values of the shift parameter, the autocorrelation being symmetric about the zero value of the parameter. The refinement is initiated via an inverse Fourier transform, here using the square root of the normalized reflectivity as the modulus and a trial phase function, to produce the first approximation to the gradient profile. Since the trial phase function is entirely arbitrary, this first approximation contains nonminimal fluctuations outside the bounded region. These are truncated and a new trial phase function is produced via a Fourier transform of the so-truncated gradient profile. This procedure is then repeated until convergence to an appropriately bounded gradient profile is achieved and the modulus square of its Fourier transform, the right-hand side of Eq. (1), matches the Fresnel-normalized reflectivity in the left-hand side of Eq. (1) to within the noise level of the latter experimental function. The trial phase function can be generated from the Fourier transform of the gradient of a density

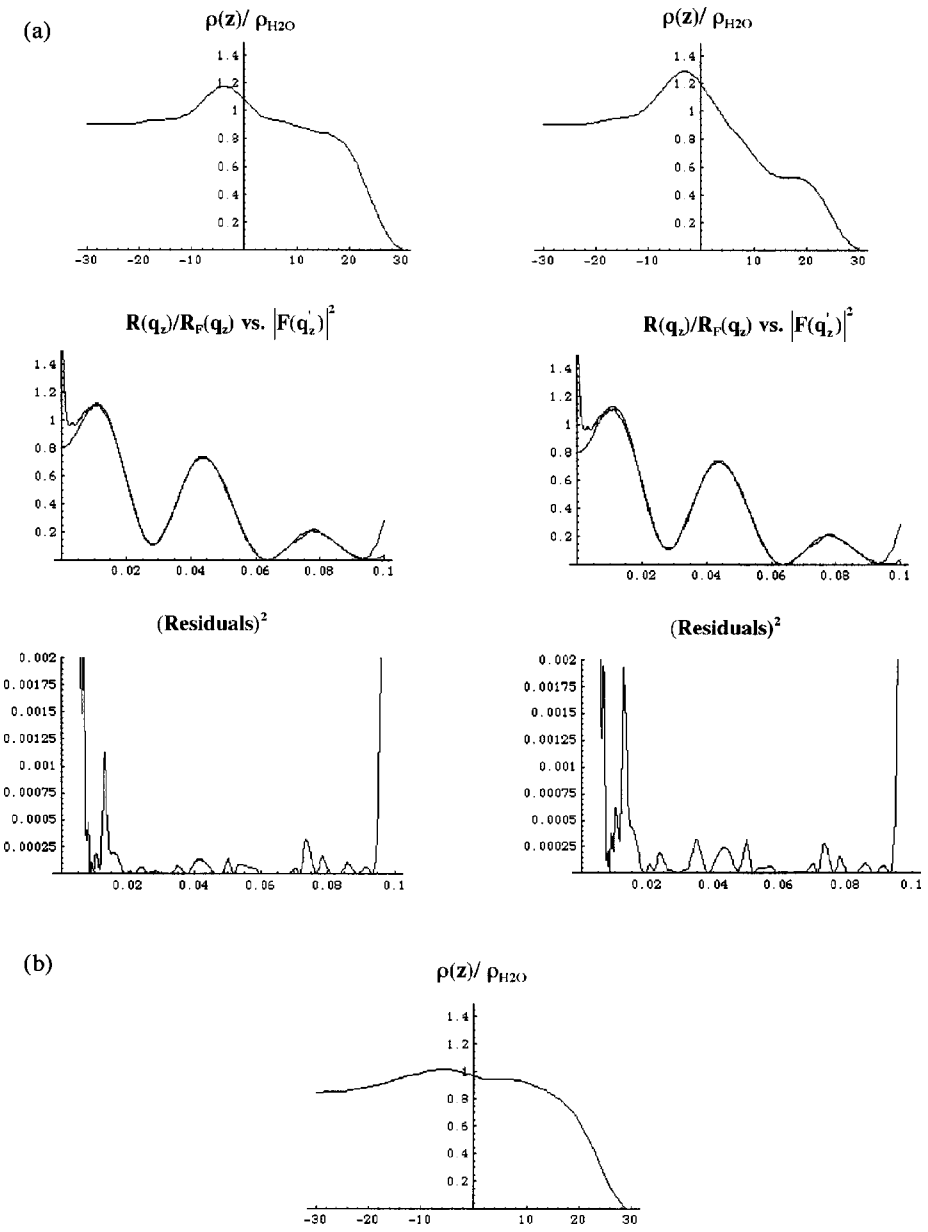

FIG. 3. (A) The two non-symmetry-related absolute electron density profiles for the pure DLgPC case are shown in the top row. The left profile for this case has a gradient profile whose Fourier transform modulus squared $|F(q_z')|^2$ agrees more closely with the experimental normalized reflectivity $R(q_z')/R_F(q_z')$ via Eq. (1), shown in the second row, than that for the right profile by a factor of 2 in terms of the magnitudes of the uniformly distributed residuals, shown in the third row. The only non-symmetry-related absolute electron density profile for the DLgPC/Vpu=10:1 mole ratio case is shown in (B).

profile for a uniform liquid with an ideally smooth surface, the gradient of a density profile that is clearly ''incorrect'' based on one's physical-chemical knowledge of the system, or the gradients of any number of otherwise totally arbitrary density profile structures. As in any refinement approach, there is no uniqueness theorem. Thus, the possibility of other non-symmetry-related solutions is best approached when phase space is otherwise systematically explored (e.g., Ref. 19), as described in the Results section. The approach described can now be easily implemented via symbolic computation such as with MATHEMATICA.

The resulting gradient SLD profile can be integrated numerically to provide the SLD profile itself, utilizing the known scattering-length density of the subphase to determine the constant of integration. However, there are errors associated with such numerical integration methods and the integration specifically requires that the gradient profile exhibit minimal amplitude fluctuations strictly about zero beyond the boundaries, as opposed to fluctuations about some small, but nonzero constant value. The latter can arise, for example, from any errors in the Fresnel-normalized reflectivity at smaller values of momentum transfer and appear similarly in the autocorrelation of the gradient profile beyond its boundary.

However, returning to the so-called ''slab model'' for the SLD profile described in the Introduction, the gradient profile $d\rho(z)/dz$ can be described by a sum of analytic Gaussian functions for each interface completely defined by the change in average scattering-length density across the interface $\Delta\rho_{j,j+1}$, its position in the profile z_j, and its width (or roughness) σ_j. Thus, the gradient profiles $d\rho(z)/dz$ determined unambiguously, utilizing the box-refinement method to solve the phase problem in the distorted-wave Born approximation, can be considered to contain a sum of Gaussian functions uniquely defining the positions of the interfaces z_j in the monolayer profile structure. One can then fit a sum of

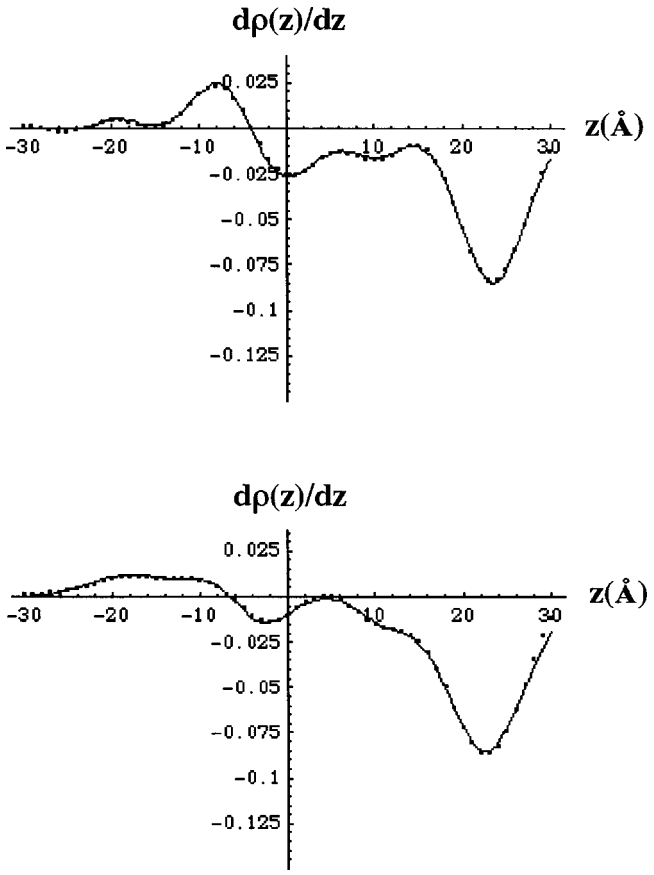

FIG. 4. Gradients of the monolayer electron density profiles $d\rho(z)/dz$ derived unambiguously from the experimental Fresnel-normalized x-ray reflectivity data via the box-refinement method, exactly as in Ref. 4, are shown as the dotted lines for the pure phospholipid DLgPC (top) and its binary mixture with an HIV-1 accessory protein Vpu at a DLgPC/Vpu mole ratio of 10:1 (bottom). The minimum representing the hydrocarbon/helium interface occurs in the region $+20$ Å$<z<+26$ Å in both monolayer profiles as shown here, which places that for the polar headgroup/hydrocarbon chain interface at the $z=0$ Å origin for the pure DLgPC case, that choice being entirely arbitrary and of no other consequence. The best nonlinear least-squares fits of the sum of five Gaussian functions to the gradients of the monolayer electron density profiles $d\rho(z)/dz$ from box refinement are shown as the solid lines.

Gaussian functions to the unambiguously determined gradient profiles $d\rho(z)/dz$ using an objective nonlinear least-squares fitting procedure, the goodness of fit provided by a combination of both the global sum of the residuals and the distribution of the residuals over the range of the profile coordinate z within the bounded region. Here, a minimum number of such Gaussian functions is sought to represent the gradient profile $d\rho(z)/dz$ sufficient to make (a) the modulus squared of its Fourier transform match the experimental normalized reflectivity data via Eq. (1) and (b) the analytic integration of the sum of Gaussian functions fitted to the gradient profile $d\rho(z)/dz$ match the absolute SLD profile $\rho(z)$ obtained by numerical integration of the gradient profile $d\rho(z)/dz$.

The gradient profiles $d\rho(z)/dz$ determined unambiguously via the box-refinement method necessarily exhibit the effects of Fourier transform truncation, namely, they contain a low amplitude, minimum wavelength component throughout determined completely by the largest value of q_z with which significant specular reflectivity data are observed.[4] Clearly the larger maxima and minima in these gradient profiles arise from the positions of the dominant interfaces in the monolayer profile structure. One can find the positions of these maxima and minima by simply differentiating the gradient profile and solving for the z positions of the zeros. We note that these positions obtained with this approach are not exactly the same as those found via the fitting of a sum of Gaussian functions to the gradient profile because the positions of neighboring Gaussians can be affected by their respective widths relative to their separation. However, the resulting so-fitted sum of Gaussian functions to the gradient profile is very appealing because it allows for its analytic integration to accurately provide the absolute SLD profile $\rho(z)$ itself for the monolayer. Importantly, this analytic integration provides the absolute scattering-length density profile $\rho(z)$ in precisely the terms employed in the less unambiguous slab-model refinement, namely, in terms of layers (or "slabs") of average density $\overline{\rho_j}$ bounded by the two interfaces z_j and z_{j+1} of widths (or roughnesses) σ_j and σ_{j+1}.

Both the method of steepest descents and the Levenberg-Marquardt algorithm have been utilized to effect the nonlinear least-squares fitting, as provided for example in MATHEMATICA. As is generally the case, given the large number of parameters required to describe even a small number of interfaces at three parameters per interface, it is often necessary to perform a so-called grid search for some of the parameters, allowing the remainder to float in order to best minimize the goodness of fit. It should be noted that the fitting of Gaussian functions to a particular region of the gradient profile can generally be localized only to that region of the gradient profile. Only when a Gaussian has an unusually large amplitude coupled with an unusually broad width can it affect the fitting of Gaussian functions to more distant regions of the gradient profile. This is because the phase problem has been solved and the fitting is performed in real space. In direct contrast, in the slab-model refinement procedure traditionally employed, the parameters defining any particular interface are delocalized throughout momentum transfer space, which increases the coupling between the parameters to be determined.

RESULTS

Some key results are shown here for Langmuir monolayers of binary mixtures of an HIV-1 accessory protein Vpu and a diacylphospholipid DLgPC over a range of mole ratios taken from Refs. 4 and 20. Figures 1A–H show all of the functions employed in deriving the gradient SLD (i.e., electron density) profiles from the Fresnel-normalized x-ray reflectivity data via box refinement and their numerical integration to provide the absolute electron density profiles for two monolayers at the extremes of mole ratios investigated. In this example, the iteration for both monolayers was initiated with the phases (Figure 1C) for the same gradient SLD profile (Figure 1A), which could not be correct for either,

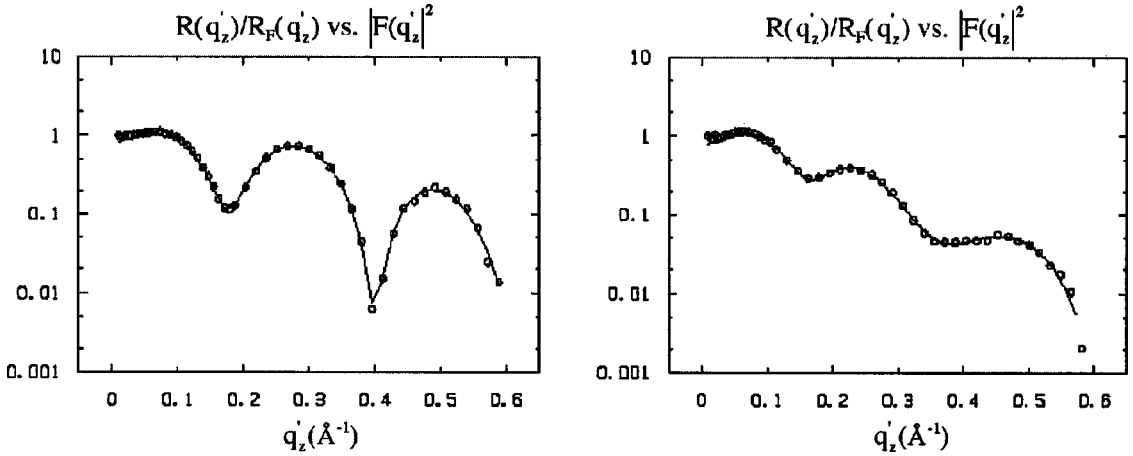

FIG. 5. Criterion (a): Experimental Fresnel-normalized reflectivity data are shown as dotted lines for pure DLgPC (left) and its binary mixture at a DLgPC/Vpu mole ratio of 10:1 (right) and $|F(q_z')|^2$, calculated via Eq. (1) for the best nonlinear least-squares fits of the sum of five Gaussian functions to the gradients of the monolayer electron density profiles $d\rho(z)/dz$ from box refinement, are shown as the solid lines.

based on one's prior independent knowledge of these monolayer systems. The corresponding trial gradient profile is not shown here.

Given the maximum possible extents of the gradient SLD profiles based on their respective autocorrelation functions shown in Figure 1E, a set of trial gradient SLD profiles were generated to represent the full range of gradient profiles from totally symmetric (even) to totally antisymmetric (odd), as shown in Figure 2A, whose Fourier transforms would possess a modulus that varied as rapidly as physically possible and a phase that sampled all of phase space within the range of $\pm\pi$ over the range of momentum transfer q_z accessed, as shown in Figure 2B. Neglecting for the moment the obviously equivalent, symmetry-related solutions to Eq. (1) for the gradient SLD profiles $d\rho(z)/dz$, namely, $-d\rho(z)/dz$, $d\rho(-z)/dz$, and $-d\rho(-z)/dz$ since they possess the same Fourier transform modulus, only two distinct solutions were obtained for the pure DLgPC case. One predicted the experimental normalized reflectivity (Figure 3A, middle) with uniformly distributed residuals smaller by a factor of 2 compared with the other (Figure 3A, bottom). The numerical integrals of these two possible solutions, namely, the corresponding SLD profiles $\rho(z)$, are shown in Figure 3A, top, left-hand side and right-hand side, respectively. Given the noise level due to the counting statistics in the experimental data where these differences in the residuals occur for the two possible solutions, the one corresponding to the SLD profile shown on the right-hand side may be rejected on this basis alone. We note that since the normalized reflectivity data and the autocorrelation of the gradient SLD profile are related by a unique Fourier transform, the differences in the residuals for the two possible solutions shown in Figure 3A, bottom, should also be manifest in the corresponding autocorrelation functions as well. Only one solution was obtained for the DlgPC/Vpu=10:1 mole ratio case whose corresponding SLD profile is shown in Figure 3B. Since these SLD profiles contain a region whose SLD is greater than that of the subphase, the equivalent symmetry-related solutions $-d\rho(z)/dz$ and $-d\rho(-z)/dz$ are not physically reasonable, as they require that region to possess negative SLD, which is not possible for the x-ray case. The remaining symmetry-related solution $d\rho(-z)/dz$ is trivially related to $d\rho(z)/dz$ because the average SLD values over the two regions outside the boundaries of the gradient SLD profile, where $d\rho(z)/dz$ is zero, are known.

In Ref. 20, the best fits of four Gaussian functions, representing four interfaces defining three layers (or slabs) within the profile structure, to the gradient electron density profiles determined via box refinement for the same two monolayers at the extremes of mole ratios (shown as dotted lines in Fig. 4) were obtained. Here, the Gaussians were fitted to the four maxima/minima in the gradient profiles within the region $-15\ \text{Å}<z<30\ \text{Å}$ ignoring the maximum at $z\approx-20$ Å for both monolayers. Nevertheless, the best fits for these two cases satisfy to a large extent the criteria (a) the modulus square of its Fourier transform matching the experimental normalized reflectivity data via Eq. (1) and (b) the analytic integration of the sum of Gaussian functions fitted to the gradient profile $d\rho(z)/dz$ matching the absolute electron density profile $\rho(z)$ obtained by numerical integration of the gradient profile $d\rho(z)/dz$. Including the maximum at $z\approx20$ Å but ignoring the minimum at $z\approx10$ Å for both monolayers in the best fits of only four Gaussian functions to the gradient profiles, results in criterion (a) being satisfied to a significantly lesser extent. Perhaps not surprisingly, both nonlinear least-squares fitting algorithms mentioned above failed, attempting to utilize five Gaussian functions described by 15 parameters.

In Fig. 4, these best four-Gaussian fits were combined, easily providing with only minor adjustments guided by least-squares minimization, the best fits of five Gaussian functions (shown as solid lines) to the gradient SLD profiles determined via box refinement for the same two monolayers at the extremes of mole ratios investigated. These best fits satisfy both criteria exactly, including criterion (a) to within the noise level throughout the range of momentum transfer Q_z investigated, as shown in Figs. 5 and 6. The parameters

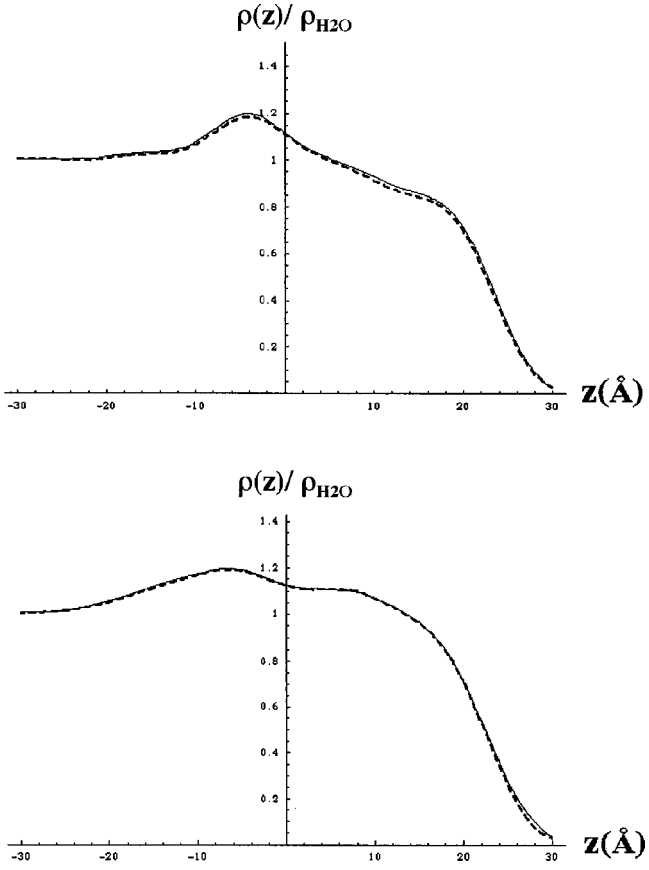

FIG. 6. Criterion (b): The absolute electron density $\rho(z)$ profiles calculated by *analytic integration* (solid lines) of the best nonlinear least-squares fits of the sum of five Gaussian functions to the gradients of the monolayer electron density profiles $d\rho(z)/dz$ from box refinement for the case of pure DLgPC (top) and its binary mixture at a DLgPC/Vpu mole ratio of 10:1 (bottom). The absolute electron density $\rho(z)$ profiles calculated by *numerical integration* of the gradients of the monolayer electron density profiles $d\rho(z)/dz$ from box refinement appear as dotted lines.

of the five Gaussians are given in Table I and the analytic integration of the gradient profiles to the absolute SLD (electron density) profiles for these same two monolayers is shown in Fig. 6. It may be noted that from Table I, it is apparent that the $\Delta\rho$'s for the DLgPC/Vpu=10:1 mole ratio case satisfy one criterion in Ref. 12 necessary to produce a unique solution, namely, that the magnitude of $\Delta\rho$ for one interface be greater than the sum of the $\Delta\rho$ magnitudes for the others, although the other criterion that the interfacial roughnesses be small is clearly not met. In contrast, neither criterion is satisfied for the pure DLgPC case, although one solution is clearly favored over the other, provided the counting statistics errors on the normalized reflectivity data are sufficiently small.

DISCUSSION

The so-called box-refinement approach utilizes a powerful boundary condition that can be determined unambiguously from the experimental normalized reflectivity data, to solve the phase problem. It is important to note that its precise value is not important, only that the boundary condition imposed in the iterative refinement not be smaller than the actual bounds of the gradient SLD profile. It has been shown that the bounded nature of the gradient SLD profile is sufficient to provide a solution to the phase problem for the Fresnel-normalized specular x-ray or neutron reflectivity from a liquid surface or from a thin film on a liquid surface in the distorted-wave Born approximation. Phase space can furthermore be systematically explored to investigate the possibility of other solutions, symmetry related or not. Nonsymmetry-related solutions can be rejected on the basis of the two criteria provided herein, depending mostly on the accuracy of the normalized reflectivity data over the range of momentum transfer accessed, provided that the distorted-wave Born approximation is satisfied. Symmetry-related solutions can only be rejected on the basis of independent knowledge of the system, e.g., physical or physical-chemical such as the non-negative electron density in the x-ray case. Otherwise, the box-refinement approach is more general in that it can be shown to provide unique solutions under conditions that are not sufficient for the approach based on the logarithmic dispersion relations for Fourier transforms. However, neither approach is as powerful as that available for phasing the specular x-ray or neutron reflectivity from thin films on solid substrates. In such cases, the solid substrate can be tailored synthetically to provide a reference structure for interferometric phasing, whether or not the distorted-wave Born approximation is satisfied,[15–17,21] and the solutions are shown to be unique. Unfortunately, the presence of the solid substrate may perturb the system of interest in which case the box refinement and to a lesser extent the logarithmic dispersion relation approaches are superior to the slab-model refinement approach in that the phase problem is solved.

TABLE I. Parameters from the best five-Gaussian fits to the gradients of the monolayer electron density profiles shown in Fig. 4. The absolute electron density profiles constructed from these parameters appear in Fig. 6 as dotted lines. Note that $\rho_1=\rho_{subphase}=0.333e^-/\text{Å}^3$ and $\rho_6=\rho_{\text{He}}\approx 0.000e^-/\text{Å}^3$.

Monolayer	j	z_j (Å)	σ_j (Å)	ρ_{j+1} ($e^-/\text{Å}^3$)	$\Delta\rho_{j,j+1}$ ($e^-/\text{Å}^3$)
DLgPC	1	−19.106	2.028	0.345	+0.012
	2	−6.750	3.321	0.471	+0.126
	3	−2.005	4.578	0.319	−0.152
	4	10.327	2.904	0.282	−0.037
	5	23.464	3.661	0.001	−0.281
DLgPC:Vpu=10:1	1	−18.050	4.593	0.382	+0.049
	2	−8.996	3.002	0.403	+0.021
	3	−2.851	2.901	0.365	−0.038
	4	11.427	2.904	0.329	−0.036
	5	22.476	4.337	0.001	−0.328

ACKNOWLEDGMENTS

This work was supported by research grants from the National Institutes of Health (P01-GM56538 and P01-GM55876) and the National Science Foundation (DMR00-79909). The x-ray reflectivity data were collected at the National Synchrotron Light Source (beamline X22B) and the Advanced Photon Source (Sector 09; Complex Materials Consortium), supported by the Department of Energy, Basic Energy Sciences.

[1] X.L. Zhou, Phys. Rev. E **52**, 1938 (1995).
[2] H. Tostmann, E. DiMasi, O.G. Shpyrko, P.S. Pershan, B.M. Ocko, and M. Deutsch, Phys. Rev. Lett. **84**, 4385 (2000).
[3] J. Als-Nielsen, D. Jacquemain, K. Kjaer, F. Leveiller, M. Lahav, and L. Leiserowitz, Phys. Rep. **246**, 251 (1994).
[4] S. Zheng, J. Strzalka, C. Ma, S.J. Opella, B.M. Ocko, and J.K. Blasie, Biophys. J. **80**, 1837 (2001).
[5] J. Majewski, T.L. Kuhl, K. Kjaer, and G.S. Smith, Biophys. J. **81**, 2707 (2001).
[6] R. Hosemann and S.N. Bagchi, *Direct Analysis of Diffraction by Matter* (North-Holland, Amsterdam, 1962).
[7] W. Lesslauer and J.K. Blasie, Acta Crystallogr., Sect. A: Cryst. Phys., Diffr., Theor. Gen. Crystallogr. **27**, 456 (1971); Biophys. J. **12**, 175 (1972).
[8] V. Skita, M. Filipkowski, A.F. Garito, and J.K. Blasie, Phys. Rev. B **34**, 5826 (1986).
[9] R.M. Stroud, and D.A. Agard, Biophys. J. **25**, 495 (1979).
[10] L. Makowski, J. Appl. Crystallogr. **14**, 160 (1981).
[11] J. Strzalka, X. Chen, C.C. Moser, P.L. Dutton, B.M. Ocko, and J.K. Blasie, Langmuir **16**, 10 404 (2000).
[12] W.L. Clinton, Phys. Rev. B **48**, 1 (1993).
[13] R.E. Burge, M.A. Fiddy, A.H. Greenaway, and G. Ross, Proc. R. Soc. London, Ser. A **350**, 191 (1976).
[14] K.H. Zimmermann, M. Tolan, R. Weber, J. Stettner, A.K. Doerr, and W. Press, Phys. Rev. B **62**, 10 377 (2000).
[15] J.K. Blasie, S. Xu, M. Murphy, J. Chupa, J.P. McCauley, A.B. Smith III, J.C. Bean, and L.J. Peticolas, Mater. Res. Soc. Symp. Proc. **237**, 399 (1992).
[16] L.R. Kneller, A.M. Edwards, C.E. Nordgren, J.K. Blasie, N.F. Berk, S. Krueger, and C.F. Majkrzak, Biophys. J. **80**, 2248 (2001).
[17] C.F. Majkrzak and N.F. Berk, Phys. Rev. B **52**, 10 827 (1995).
[18] V.-O. de Hann, A.A. van Well, S. Adenwalla, and G.P. Felcher, Phys. Rev. B **52**, 10 831 (1995).
[19] F.J. Asturias and J.K. Blasie, Biophys. J. **55**, 739 (1989).
[20] S. Zheng, J. Strzalka, D.H. Jones, S.J. Opella, and J.K. Blasie, Biophys. J. **84**, 2393 (2003).
[21] J.A. Chupa, J.P. McCauley, Jr., R.M. Strongin, A.B. Smith III, J.K. Blasie, L.J. Petacolas, and J.C. Bean, Biophys. J. **67**, 336 (1994).